ISS TRANSACTIONS

Laboratory Experiments on Arc Deflection and Instability

S. Zweben and M. Karasik
Princeton Plasma Physics Laboratory

ABSTRACT

This article describes experiments on arc deflection instability carried out during the past few years at the Princeton University Plasma Physics Laboratory (PPPL). Our approach has been that of plasma physicists interested in arcs, but we believe these results may be useful to engineers who are responsible for controlling arc behavior in large electric steel furnaces.

Arcs are a type of "plasma," – that is, a gas that is hot enough for some of the electrons to break free from the atoms (ionize) and conduct electricity. Arc temperatures are typically 10,000°C, which makes their electrical resistivity about 1,000 times higher than steel. This high resistance is desirable for the EAF application, in which the arc acts like a heating element in the EAF circuit. However, arcs (and most plasmas) are sensitive to deflection by magnetic fields and are generally unstable.

The behavior of arcs has been studied for many years,[1-3] but the physical causes of arc deflection and instability in industrial scale electric arc furnaces (EAFs) are not yet well-understood. This is partly due to the difficulties of making arc measurements inside an operating furnace and the intrinsic complexity of arc behavior itself.

PPPL does plasma physics research with the long-term goal of practical fusion energy production. Fusion furnaces, such as the Tokamak Fusion Test Reactor (TFTR) at PPPL[4] have plasma currents of 3 MA, diameters of 25 feet and heating powers of 40 MW, which produce a plasma temperature of up to 400,000,000°C. The horizontal and vertical location (i.e., deflection) of these plasmas is routinely controlled to well within 1 cm, and the large-scale plasma instabilities are successfully controlled during normal operation. Thus, we had reasons to believe that arc deflection and instability can be controlled, though not in exactly the same way as in fusion plasmas.

The work described in the following sections was part of a Ph.D. thesis project to understand the physics of arc deflection and instability in laboratory-scale furnaces.[5] We have not had an opportunity to do systematic measurements or experiments on an industrial scale furnace.

THE PPPL ARC FURNACE

A photo of the small PPPL arc furnace is shown in Figure 1. It has a vertically movable graphite cathode, typically three-eighths of one inch in diameter, and an iron or steel anode of 6 inch diameter. For unobstructed viewing access, no slag or shell is present, so arcs of $L \leq 10$ cm in length could be observed and photographed. The arc current was $I \leq 250$ amps with a DC power level of ≤ 30 kW, making it similar to a well-regulated DC arc welder. The arc was struck by touching the cathode to the anode and drawing the arc up. It was run in air with ventilation but without water cooling, so the duration of each run was limited to 10 to 15 minutes to avoid overheating the enclosure.

Electromagnetic coils were placed on the sides and below the furnace to study the effects of magnetic fields on the arc deflection and instability. A spatially

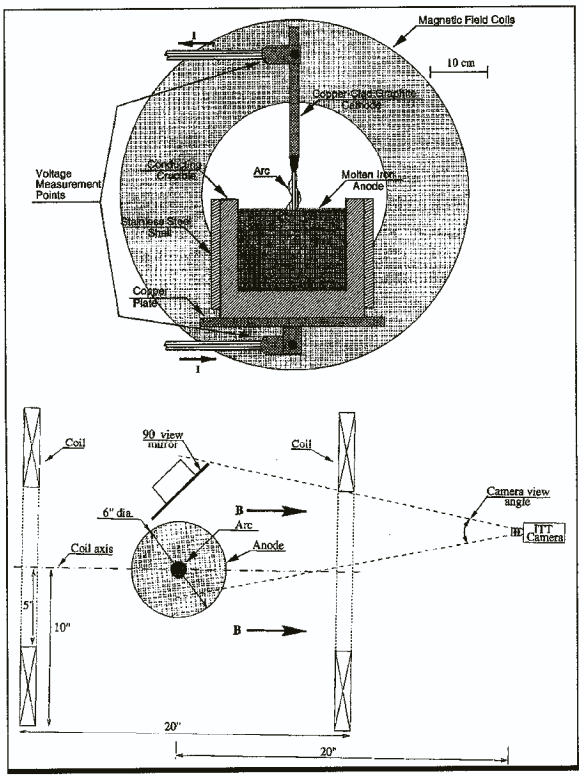

Figure 1
Schematic drawing of the PPPL arc furnace. The steel furnace anode has a diameter of 6 inches and the graphite cathode has a typical diameter of three-eighths inch. A uniform horizontal magnetic field can be imposed at the arc by the pair of 20 inch diameter coils shown. The arc is fed by a 30 kW DC supply and the cathode height can be varied during a run. The arc is viewed horizontally by a fast gated camera and at 90 degrees by a nearby mirror.

uniform horizontal magnetic field of B ≤ 10 Gauss was created at the arc with a frequency from DC to 10 kHz, as measured directly using Hall and magnetic probes when the arc current was off. A gated, intensified CCD camera was used to photograph the arc light emission at a standard TV framing rate but with a 10 μsec exposure per frame time to "freeze" the arc motion. The arc could also be viewed by eye through dark welding glass. Electrical measurements were made of the arc voltage and current from DC up to 2 kHz, and the arc location in the horizontal direction was measured with an array of fast photodiodes.

Parameters of the PPPL arc are compared with those of an industrial scale EAF furnace (Table I). Clearly some parameters are different, such as the ratio of the plasma pressure to the magnetic field pressure β and the Mach number of the arc jet flow. Therefore, caution should be used in applying these results to large furnaces, as will be discussed under *Needs for Further Research*.

ARC DEFLECTION

Undesirable arc deflection in EAFs or arc welders can be caused by the stray magnetic fields created by the electrical buswork leading to arc.[6-8] In general, the arc is deflected by the $F_x = I_z \times B_y$ force caused by the interaction of the arc current I_z and the magnetic field B_y perpendicular to the arc, where the force F_x is perpendicular to both I_z and B_y.

Typically, the arc current I_z is vertical and the magnetic field caused by the external buswork is horizontal. Thus, the $I_z \times B_y$ force tends to deflect the arc away from the furnace power supply, as illustrated in Figure 2. However, this effect can easily be modified in EAFs by the iron shell and unmelted scrap, which can shield magnetic fields from the arc itself, and by other factors, such as the foamy slag or electrode geometry. In industrial furnaces, the arc deflection angle is difficult to measure directly, and its relationship with the externally generated magnetic fields is not easy to evaluate.

In the PPPL arc deflection experiment, as described in detail in reference 9, a uniform horizontal transverse field B_y was applied to a stable vertical arc with a current I_z, always producing a clear arc deflection in the expected $F_x = I_z \times B_y$ direction, as illustrated in the CCD images shown at the top of Figure 3. The arc maintains this steady deflected position as long as a steady transverse B_y field is applied. The parameters for Figure 3 were B = 2 Gauss and I = 150 A, corresponding to a force on the arc of $F_x \approx 3 \times 10^{-2}$ N/m, or about 2×10^{-3} kg of force for an arc of length L ≈ 0.07m.

The simplest theoretical analysis of such arc deflection assumes the arc behaves like a thin wire with current I_z and linear mass density m (kg/m), acted on by the uniform transverse force $I_z \times B_y$ (N/m). The boundary conditions for this experiment are that the arc is fixed at the cathode and freely movable at the anode. A crucial element of this analysis is the arc jet speed v_z (m/second), which is assumed here to be a constant along the axial direction z of the arc (see the following). With these assumptions, the deflected shape of the arc in the $I_z \times B_y$ or x direction is a parabola:[9, 10]

$$x = [IB / (2mv_z^2)]z^2 = Dz^2 \quad .....(1)$$

In this equation, the arc deflection coefficient $D = [IB/(2mv^2)]$ can be interpreted as the ratio of the transverse driving force per unit length $I_z \times B_y$ to the arc jet kinetic energy per unit length $mv_z^2/2$. Thus, the transverse arc deflection "x" at a given distance from the cathode "z" increases linearly with I_z and B_y. Good fits of the observed arc shape to this parabolic model are obtained in the experiment, as shown at the bottom of Figure 3.

The arc in this analysis acts like the jet from a water hose being blown in the wind – the deflection depending on the force of the wind – but also on the

Table I Approximate Arc Parameters for the PPPL Furnace (left) and a 100 MW Industrial Scale DC Furnace (right)

Parameter	*Definition*	*Magnitude* *PPPL Arc*	*Industrial Arc*
Power (peak)	VI	25 kW	100 MW
Temperature	$T_e = T_i = T_n$	1 eV	1-2 eV
E-field (arc column)	E	10 V/cm	10 V/cm
Current (peak)	I	250 A	100 kA
Self B-field	B_{self}	200 G	6 kG
Pressure	$p = nkT$	1 atm	≥ 1 atm
e^- Density (peak)	n_e	10^{17} cm^{-3}	≥ 10^{17} cm^{-3}
Characteristic arc diameter	L	.6 cm	10 cm
Cathode spot radius	r_c	1.3 mm	2.5 cm
Ionization fraction (%)	n_e/n	~ 10%	10 to 100%
Debye length	$\lambda_D = \sqrt{\frac{kT\,\epsilon_0}{4\pi n_c^2}}$	10^{-6} cm	10^{-6} cm
Plasma parameter	$(4\pi/3)n_e\lambda_D^3$	~ 5	~ 5
Plasma frequency	$f_{pe} = \sqrt{\frac{n_c e^2}{4\pi^2\,\epsilon_0\,m_c}}$	10^{12} Hz	10^{12} Hz
Ion gyrofrequency	$f_{ci} = \frac{eB_{self}}{2\pi m_i}$	10^4 Hz	10^5 Hz
Ion gyroradius	$\rho L_i = \frac{\sqrt{kT/m_i}}{2\pi f_c i}$	2 cm	.6 mm
e^- Collision frequency	$\nu_e = \frac{n_i e^4 \ln\Lambda/\pi^2\,\epsilon_0^2}{12\sqrt{2m_c}(kT_c)^{3/2}}$	10^{11} sec^{-1}	10^{11} sec^{-1}
e^- Mean free path	$\lambda_{mfp,e} = \frac{\sqrt{kT/m_c}}{\nu_c}$	10^{-5} cm	10^{-5} cm
Conductivity	$\sigma = (I/\pi L^2)/E$	80 Ω^{-1} cm^{-1}	100 Ω^{-1} cm^{-1}
Resistive	$\tau_R = \mu_0 L^2 \sigma$	10^{-7} sec	10^{-4} sec
Alfvén speed	$V_A = B_{self}/\sqrt{\mu_0 \rho}$	10^4 cm/s	10^5 cm/s
Magnetic Reynolds No.	$R_m = \tau_R V_A / L$	10^{-3}	~ 1
Plasma β	$\beta = \frac{p}{(B_{self}^2/2\pi\mu_0)}$	~ 1,000	~ 1
Plasma jet speed (peak)	$\upsilon_{jet} = I\sqrt{\frac{\mu_0}{2\pi^2 r_c^2 \rho}}$	10^4 cm/s	10^5 cm/s
Mach number (peak)	M	10^{-2}	~ 1
Hydrodyn. Reynolds No.	$R_H = u_{jet}\, r_c/\eta$	10	10^3

mass density and speed of the water jet. Thus, the magnitude of the arc deflection cannot be determined from I_z and B_y alone, but also requires a knowledge of both m and v_z. These parameters are difficult to measure directly in the small PPPL furnace (and even more difficult to measure in an industrial furnace).

A theory for determining the arc jet velocity was developed in the classic work of Maecker[11] and has been qualitatively verified in some controlled experiments.[1-3] The arc jet velocity is caused by a narrow constriction of the arc near the graphite cathode (the cathode "spot"), which is small because of the high temperature required for the cathode to emit electrons. This arc constriction at the cathode spot increases the local self-magnetic field, which causes a radially inward magnetic pressure on the arc. The high collisionality of the arc causes the pressure to be transferred into the axial direction, which causes the plasma jet velocity to be directed down the length of the arc. This type of magnetic "pinch" is familiar in plasma fusion research and is somewhat similar to the jet of water created by squeezing a plastic container with a narrow spout.

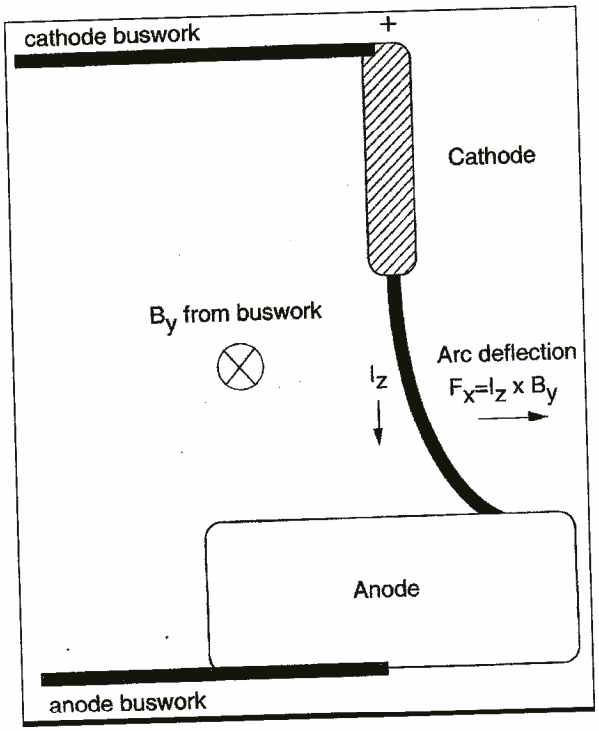

Figure 2
A diagram of arc deflection in a DC furnace. The arc current I_z is acted upon by a force $F_x = I_z \times B_y$ because of the magnetic field created by the buswork B_y. This causes the arc to be deflected away from the power supply. This model ignores the effect of magnetic material around the furnace, which may be important in practice.

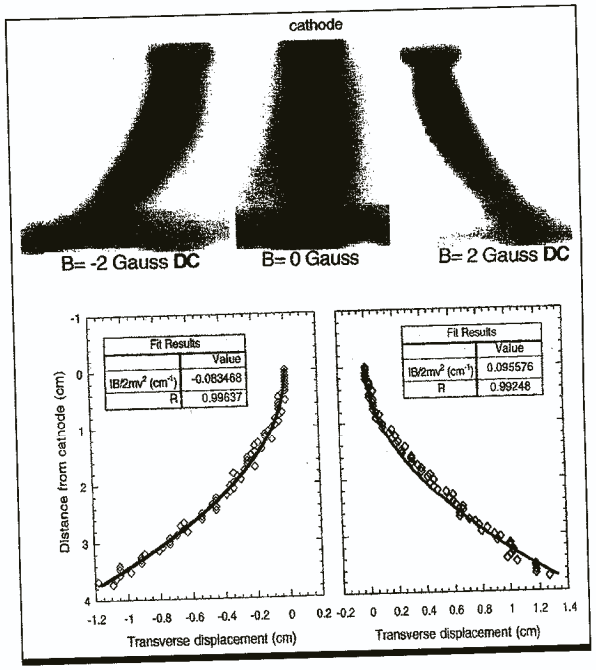

Figure 3
Arc deflection caused by externally applied DC magnetic fields. The photos at the top are negatives of CCD images of the arc deflection for two different transverse DC magnetic fields (± 2 Gauss). The arc is about 4 cm in length and connects the graphite cathode with the molten steel anode. These pictures were taken with a 10μsec exposure time and compressed vertically by 2.4:1. At the bottom are fits between the digitized shape of these arcs and the model of Equation (1). These arcs fit the parabolic shape of Equation (1) and were used to determine the arc deflection coefficient $D = [IB/2mv^2]$.

The maximum arc jet velocity near the cathode was derived by Maecker, as follows:[3, 11]

$$v_{z,max} \approx I(\mu_o / [2\pi^2 \rho r_c^2])^{1/2} \quad .....(2)$$

where r_c is the radius of the constricted arc at the cathode and ρ is the mass density of the arc per unit volume. This maximum velocity can be estimated using a typical arc current density of 3×10^7 A/m² [1, 2] (i.e., $r_c \approx 0.1$ cm at I = 150 A, and an assumed arc density corresponding to atmospheric pressure air at 10,000°C (i.e., $\rho \approx 1.7 \times 10^{-2}$ kg/m³. The velocity from Equation (2) is then $v_{z,max} \approx 300$ m/second. Note that this is the peak jet speed at the cathode spot, not the average jet speed downstream, which can be slower because of mixing with air.

In this experiment, the arc jet velocity was measured indirectly [i.e., without using Equation (21)] by forcing the arc to oscillate transversely using an AC excitation of the external magnetic field coils shown in Figure 1. The arc jet velocity can then be inferred by measuring the wavelength of the resulting deflection pattern, similar to the way in which the velocity of a water jet can be measured by oscillating the position of the hose at a known frequency.

Some examples of the arc shapes in these AC deflection experiments are shown in Figure 4, for external magnetic field strengths in the range $B_y \approx 3$ Gauss and driving frequencies in the range ≈ 500 to 1,000 Hz. The arc was seen to wriggle in the plane perpendicular to the applied $B_y(t)$ in a regular and repeating pattern. The amplitude of the AC arc deflection increases with the magnitude of the applied B_y, and the wavelength of the deflection decreases as the frequency and arc current increase. Note that the arc speed is still predominantly in the z-direction, but now the x-deflection at a given z-position oscillates in time because of the externally applied $B_y(t)$.

Digitized images of the arc shapes, such as those shown in Figure 4, were interpreted using a generalized form of the are deflection model of Equation 1, in which the spatially uniform magnetic field causing the $I_z \times B_y$ deflection is assumed to oscillate at a frequency $f = 2\pi\omega$. The solution for the arc shape is then a growing sinusoid:[9]

$$x(z,t) = (IB / m\omega^2)[\cos(\omega t - \omega z / v) - \cos(\omega t) - (z\omega / v)\sin(\omega t - \omega z / v)] \quad .....(3)$$

This solution reduces to Equation (1) for $\omega z/v_z << 1$ (i.e., the arc shape is only parabolic when the driving frequency is much less than the transit time of the arc jet from the cathode to the anode).

Figure 5 shows examples of how the experimental data, like that in Figure 4, was fit to the theoretical model of Equation (3). Such fits uniquely determine the two parameters m and v_z for a given I and B(ω). The results for our standard I = 150 A are were $m = 5 \pm 1 \times 10^{-6}$ kg/m and $v_z = 23 \pm 2$ m/second. This experimentally inferred linear mass corresponds to an arc temperature of about 7,000°C for the visually observed arc column radius of ≈ 0.7 cm, which is reasonably close to the temperature measured for this type of arc.[2, 3, 12] This inferred a jet velocity of only about one-tenth of that predicted from the theory of Equation (2), but is not unreasonable, since Equation (2) refers to the maximum jet speed near the cathode spot, and the measurement reflects the average speed along the whole arc column.

As a further check of this model, the left portion of Figure 6 shows the dimensionless form of the transverse deflection in Equation (3), namely $M = [(IB/\omega)/mv_z]$, as a function of the magnitude of the applied magnetic field. This parameter M corresponds to the ratio of the transverse momentum imparted by the $I_z \times B_y$ force in a time $(1/\omega)$ to the axial momentum of the jet. The linearity of this relationship confirms that the observed AC deflection scales linearly with the applied field [i.e., the product mv_z inferred from these fits to Equation (3) and is independent of the applied field] as expected. The right side of Figure 6 shows the inferred jet velocity v_z for varying applied frequencies, which is constant, as expected, since the axial jet speed is determined at the cathode. For this value of jet velocity and a typical electrode separation, the low frequency parabolic solution is obtained for $\omega < 575$ seconds^{-1} (i.e., below a frequency of 90 Hz, which is also consistent with the experimental observations).

In summary, the two experimental parameters m and v_z needed in the DC arc deflection model of Equation (1) were indirectly determined by applying an externally oscillating magnetic field to the arc and then fitting the resulting arc shapes to the AC arc deflection model of Equation (3). Using these parameters, we can explain the magnitude and shape of the DC arc deflection for a given externally applied DC magnetic field.

These results imply that the DC deflection of an industrial scale arc, caused by a known externally generated magnetic field, cannot be predicted without an independent knowledge of the effective arc mass density and jet velocity, which are difficult to measure directly. Possible applications of this result to industrial-scale furnaces will be discussed under *Potential Application to Industrial Furnaces.*

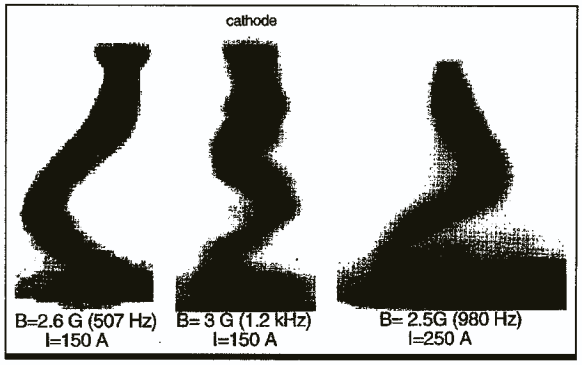

Figure 4
Sample images of the externally driven oscillatory motion of the arc at different frequencies and applied AC magnetic fields. The geometry and camera setup is the same as Figure 3. The axial wavelength is shorter for higher applied frequencies, as shown by the comparison between the left and middle images, and the wavelength increases with increasing current, as shown by the comparison between the middle and right images. At each vertical position, the arc oscillates horizontally in time at the applied frequency.

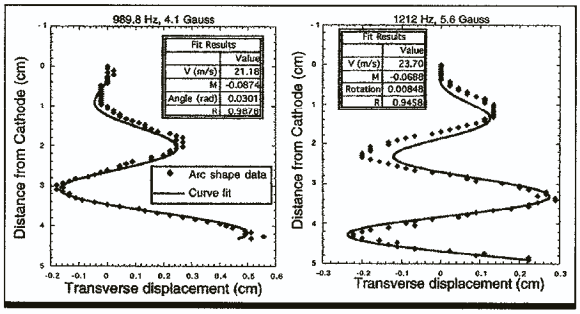

Figure 5
Examples of experimentally obtained arc shapes fit by the AC arc deflection model of Equation (3). From these fits, both the arc speed and linear mass density can be inferred. The horizonal scales are enlarged as shown, and the arc current is 150 A in both cases.

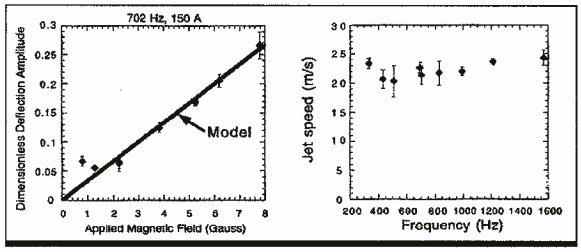

Figure 6
On the left is the relationship between the externally applied AC magnetic field and the magnitude of the arc deflection coefficient inferred from a fit of the arc shapes to the model of Equation (3). The good fit with the model implies that the arc deflections increase linearly with the applied field, as expected. On the right is the arc jet speed inferred from fits to the same model as a function of the applied AC frequency. The inferred speed is about the same at all frequencies, since the speed is determined by the arc jet.

ARC INSTABILITY

Arc instability refers to any rapidly fluctuating arc shape that occurs spontaneously, independent of any externally driven arc deflection. It is well-known that both

DC and AC industrial-scale arc furnaces are highly unstable even during their "flat bath" state after the metal scrap is melted. The arc instability generates the loud broadband acoustic noise around the furnace, with frequencies below 50 Hz to above 1,000 Hz.[13] Many attempts have been made to characterize and understand this instability.[14-19] However, the undesirable power line "flicker" caused by arc instability is generally controlled using external reactances, rather than by directly stabilizing the arc itself.

The small PPPL arc furnace was also strongly unstable in operation regimes, so a separate set of experiments was performed to identify the cause of this instability. For these experiments, the arc experiment was the same as previously mentioned under *Arc Deflection*, but no external magnetic field was applied. A detailed description of these results can be found in Reference 20. As with the deflection experiments described earlier, caution must be used in applying our results to industrial-scale furnaces (see *Potential Application to Industrial Furnaces*).

A typical case of arc instability is illustrated in Figure 7. This arc was initially stable, but after about 1 minute of burning, the arc began to "whistle" audibly and formed a conical shape as viewed by eye. In this case, the instantaneous shape of the unstable arc (as viewed with the 10 μsec exposure-time camera) was a three-dimensional helix nearly fixed at the cathode and rotating in a few-cm diameter circle at the anode. The fundamental frequency of the arc motion was measured by a linear array of fast photodiodes to be ≈ 600 Hz, with a typical waveform, as shown in Figure 8. Also shown are waveforms of the measured arc current and voltage, which also oscillated at this frequency.

The onset, amplitude, shape and frequency of this arc instability varied considerably, depending on the arc current, electrode separation and cathode geometry in this experiment.[5, 20] For example: (a) for the normal three-eighths inch diameter cathode, the instability was never observed below I = 100 A, and almost always occurred at I = 250 A; (b) its fundamental frequency was as low as ≈ 100 Hz near I = 100 A and as high as 800 kHz near I = 250 A, but had a considerable variation at each current; and (c) the arc instability sometimes became turbulent, with a broadband frequency spectrum extending from 1 Hz to 10 kHz, particularly when its amplitude was large.

However, the strongest factor that determined whether the arc was unstable or stable was the cathode geometry. The influence of the cathode geometry on arc instability has been observed before,[1, 14, 15] but apparently without a quantitative model relating it to the arc shape, which is discussed in the following section.

The clearest example of this cathode geometry effect is illustrated in Figure 9, which shows the arc shape for five different times during a single run with a "necked" graphite cathode of varying diameter. This

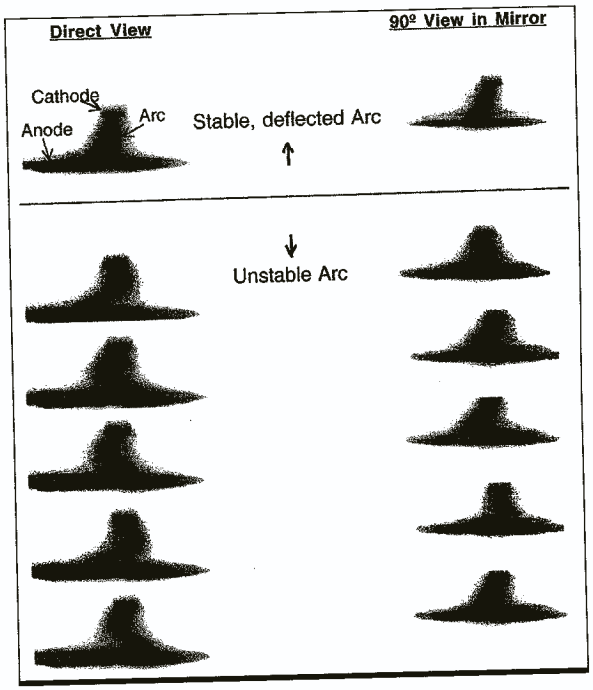

Figure 7
Sample images of an unstable arc during low amplitude oscillations. The left-hand column shows a direct view of the arc from the CCD camera, while the right-hand side shows the same arc in the 90 degree view angle mirror. The five unstable frames were picked from a 30-frame data set to illustrate the different arc column shapes. These images were each exposed for 10 μsec, and the cathode-anode gap is 3.1 cm. The horizontal scales are expanded by a factor of 2.4:1 on the left and 2.3:1 on the right.

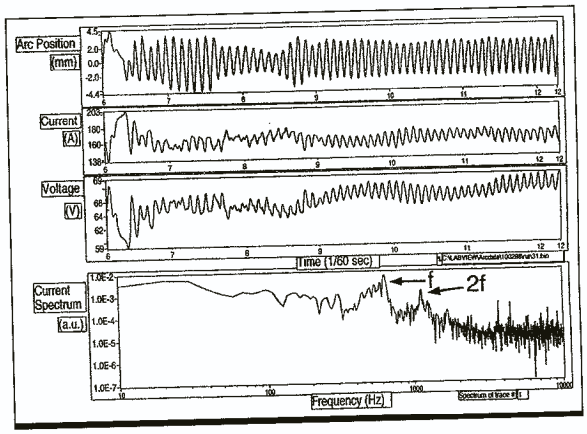

Figure 8
Time dependence of arc parameters during a low-amplitude 600 Hz arc instability. The time scale is marked in units of one-sixtieth of a second, corresponding to CCD camera frames taken at the same time. The arc position is determined from a horizontal linear array of photodiodes viewing the arc at a fixed distance above the anode. Both the arc current and voltage show few-percent fluctuations at the fundamental frequency of 600 Hz. The frequency spectrum of the current and voltage also show power at the second harmonic, as shown at the bottom.

I = 250 A arc was normally unstable for our standard three-eighths inch diameter graphite cathode, but whenever the cathode burned down to the smaller-diameter "necked" regions, the arc suddenly became stable. In fact, for cylindrical cathode shapes, the I = 250 A arc was only unstable over a certain range of cathode areas from 20 to 30 mm^2, as shown in Figure 10. For cathodes below and above this area, the I = 250 A arc was stable for all arc lengths.

One other example is useful to motivate the model for arc instability. When the graphite cathode was made into a "paddle" shape 25 mm wide by 4 mm thick, as shown in Figure 11, the wriggling arc motion was localized in the plane of the paddle rather than in a cone, as for the cylindrical cathode in Figure 7. Thus, both the onset of this instability and also its unstable shape depended critically on the cathode geometry and only weakly on the arc current or arc length.

This dependence on cathode geometry suggests that this particular instability is caused by an unstable motion of the cathode attachment "spot" rather than by a magnetically driven kinking of the arc itself. In the model, the shape of the arc motion is attributed to a rapid movement of the arc attachment point at the cathode that, when combined with the arc jet velocity directed axially away from this spot, makes a wriggling pattern, which oscillates in time and space. This is somewhat analogous to the wavy pattern formed in a jet from a water hose when its nozzle is wiggled.

A mathematical model for this type of arc instability was made by assuming that the arc had a constant axial (z-directed) velocity v_z, and that the arc spot at the cathode was gyrating in a small circle in the x-y plane with a radius "a" and a frequency f = $2\pi\omega$. The shape of the arc motion is then a helix with a diameter that grows linearly with z [e.g., the shape in the (x-z) plane]:[16]

$$x(z,t) = a[\cos(\omega t - \omega z / v_z) - (z\omega / v_z) \sin(\omega t - \omega z / v_z)] \quad .....(4)$$

Note that this model shows no force on the arc. Thus, the arc mass density does not enter into this solution – the arc plasma just moves transversely with a velocity of $v_x \leq \omega a << v_z$ after it leaves the cathode spot. This solution looks similar to that for the driven arc motion in Equation (3), but actually represents a different physical situation.

Mathematical fits between Equation (4) and the digitized shapes of various unstable arcs in this experiment are shown in Figure 12. Good fits between this model and the data can be obtained using two adjustable parameters: the arc spot motion radius "a" and the arc jet velocity v_z. The arc jet velocities inferred from these fits agree to within ≈ 20 percent of those inferred from the driven arc motion as expected.

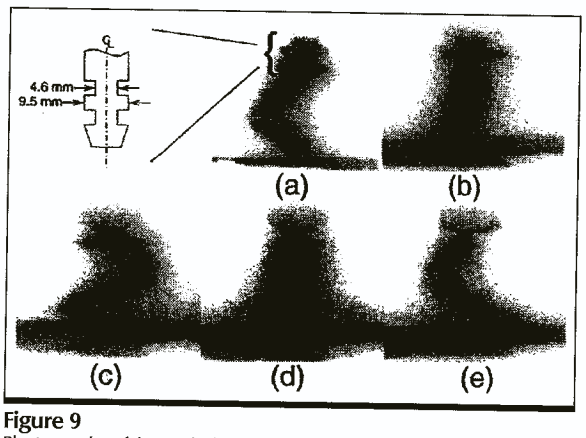

Figure 9
Photographs of the arc behavior with a "necked" cathode, in which the cathode diameter varies along the length of the cathode, as illustrated at the top left. During a single run at I = 250 A with this cathode, the arc was unstable when the cathode diameter was 9.5 mm, as shown in photos (a), (c) and (e), but was stable when the cathode was 4.6 mm diameter, as shown in photos (b) and (d). This demonstrated the effect of cathode size on arc instability in this experiment. The horizontal scale is expanded 2.4:1 in all photos.

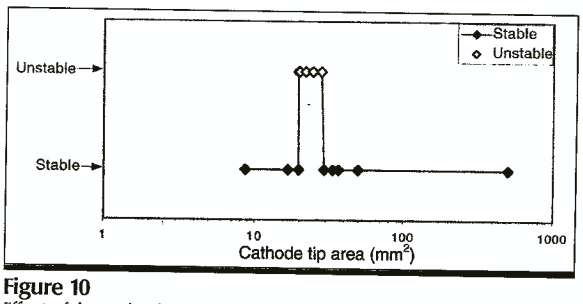

Figure 10
Effect of the cathode size on the stability of arcs in this experiment. For cylindrical cathodes, the arc at I = 25 A is unstable only for cathode areas of 20 to 30 mm^2. This illustrates the effect of cathode geometry on arc stability.

The inferred values of the cathode spot motion parameter "a" for a database of unstable arcs is shown in Figure 13, along with a few direct measurements of the visible cathode spot motion made using a magnifying lens. Both the inferred and measured cathode spot motion radii are a ≈ 0.15 ± 0.1 cm, which is comparable in size to the cathode spot itself, making this motion difficult to observe directly. The maximum transverse component of the arc velocity is therefore $v_y \approx 2\pi$ (600 Hz) (0.15 cm) ≈ 4 m/second, which causes a transverse displacement of ≈ 0.8 cm at a distance of 4 cm from the cathode, as in the data at the bottom of Figure 13. The resulting cone-shaped arc envelope is visible by eye during the arc instability.

Obviously, the next question is, what causes this unstable motion of the cathode spot? A necessary

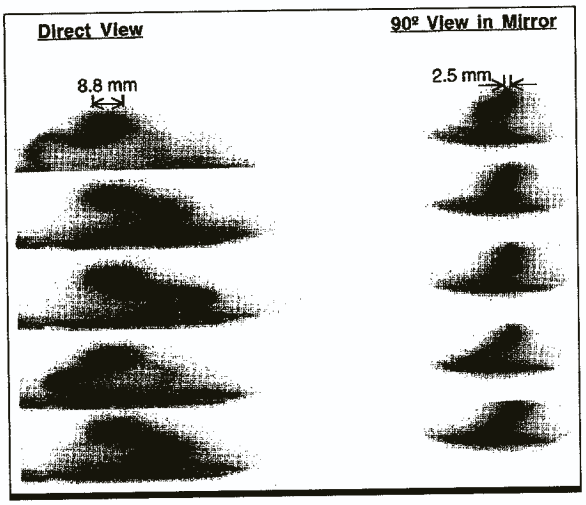

Figure 11
Sample pictures of an unstable arc during a large amplitude oscillation with a "paddle" shaped cathode, which was 8.8 mm wide by 2.5 mm thick. The left-hand column shows a direct view of the arc, and the right-hand side shows the same arc in the 90 degree view angle mirror. These images were each exposed for 10 µsec, and the cathode-anode gap is 2.7 cm. The horizontal scales are expanded by a factor of 2.4:1 on the left and 2.3:1 on the right. Note that the cathode is wider in the direct view plane and that the amplitude of arc motion is larger in this plane. Also note thatthe arc attachment is moving along the tip of the cathode.

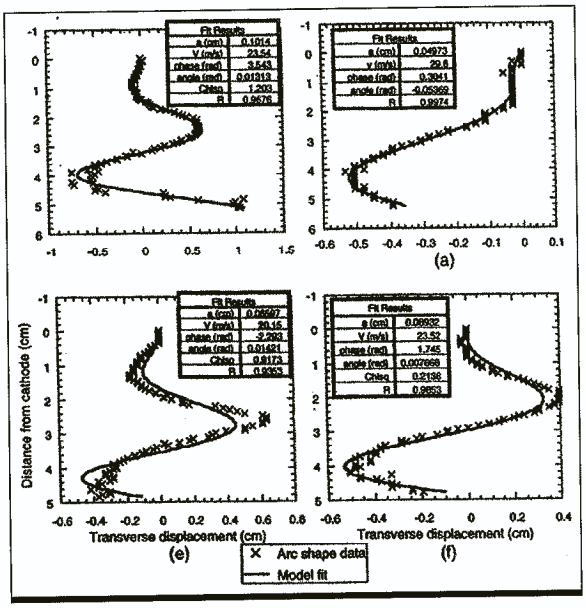

Figure 12
Examples of experimentally-obtained unstable arc shapes fit to the model of Equation (4). The "x" points are the data from arc shapes taken from digitized CCD images, and the smooth lines are solutions of the model equation. The four cases shown have arc currents and frequencies of (a) 250 A, 575 Hz; (b) 220 A, 780 Hz; (c) 197 A, 650 Hz; and (d) 222 A, 600 Hz. Note that the horizontal scales vary from case to case.

condition for cathode spot motion is that the surface temperature of the cathode must be sufficiently high

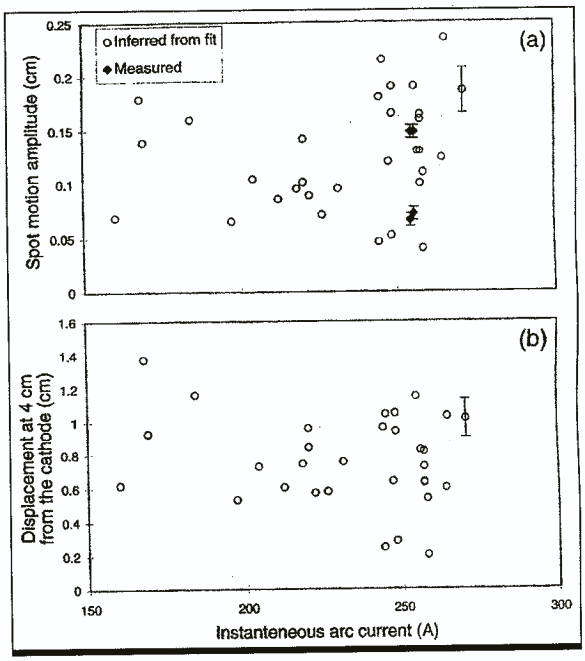

Figure 13
At the top are cathode spot motion amplitudes for unstable arcs vs. arc current. The amplitudes inferred from fits of the model to the observed arc shapes (open circles) are consistent with direct measurements of the cathode spot motion (closed diamonds). At the bottom are the maximum arc displacements measured 4 cm axially from the cathode for the same data set as the top. No apparent trend of arc displacement vs. current is evident in this range of data.

for thermionic emission to sustain the arc current (i.e., roughly ≥ 3,500°C). This can explain why the arc is unstable for only a narrow range of cathode radii (Figure 10). For larger radii, the cathode bulk cools the surface surrounding the cathode spot below this temperature, so the arc cannot move. For smaller radii, the cathode size is comparable to the cathode spot size, leaving no room to move. Within this unstable range, it is believed that some mechanism(s) is causing the cathode spot to rotate in a small circle, causing the helical arc pattern in the arc jet downstream.

However, the physical cause of the cathode spot motion in this experiment is not quantitatively understood. The mechanisms that have been evaluated,[5, 20] some of which have been considered in previous studies, are as follows:

a) Resistive heating inside the graphite cathode, caused by the arc current, increases its temperature and electrical resistivity, thus causing the internal current path to move to a cooler region of the cathode. However, the time-scale for bulk heating of a cathode volume, comparable to the cathode spot radius, would be ≈ 1 second, which would not explain the observed instability at ≈ 500 Hz.

b) Surface heating of the cathode, caused by the ion flow or radiation from the arc, could also increase its resistance locally and cause the cathode spot to move to a cooler region. However, the time scale for a significant local resistance change caused by this surface heating is similar to the estimate mentioned previously, which would not explain the observed instability at ≈ 500 Hz.

c) Cathode erosion will cause the local shape of the cathode surface to change, which could cause the arc to move. Since the arc tends to orient itself perpendicular to the cathode surface, this effect might move the arc away from any local hole caused by cathode erosion. However, the measured erosion rate of ≈ 0.06 mm/second is too small to make a significant cathode spot motion on the time-scale of the arc instability.

d) Constriction of the arc current at the cathode spot can cause a magnetic interaction between the cathode current and the arc current, resulting in an unstable equilibrium. If a slight angle is created between these currents, their magnetic interaction tends to increase this angle until the arc reaches the edge of the cathode tip at which the angle is at a maximum. The time-scale for such movement could be rapid enough to cause the instability, since the resistive diffusion time of current in the arc or cathode is small (< 10^{-5} seconds). However, it is not understood what could cause the arc to continue to move once it reaches the edge of the cathode.

e) Vaporization of the graphite at the cathode spot could cause a local cooling of the arc itself, since the neutral gas is at most 4,000°C and the arc plasma is about 10,000°C. This cooling would cause the arc's resistivity to increase, and the arc current distribution would tend to move elsewhere. The time-scale for this movement would be limited by the time to heat an adjacent area on the cathode surface to 4,000°C, which is estimated to be ≈ 10^{-3} seconds for the energy flux of ≈ 10^{8} W/m² estimated at the cathode surface. This mechanism could produce a cathode spot velocity of up to 100 m/second, which is more than enough to explain the inferred spot velocity of 4 m/second.

In summary, the arc instability for this experiment seems to be caused by a small transverse motion of the arc attachment spot at the cathode surface, and not by a magnetic or aerodynamic instability of the arc itself. This model explains the observed conical shape of the unstable arc and also the sensitivity of its onset and shape to the cathode size and shape. However, further experiments and analysis are needed in order to understand the mechanism of the arc motion at the cathode, which presumably causes this instability (see *Needs for Further Research*).

POTENTIAL APPLICATION TO INDUSTRIAL FURNACES

This section describes some potential applications of these results to industrial-scale EAFs. Here, it will be assumed that the mechanisms of arc deflection and instability are similar to those in the small experiment. This is a debatable assumption, considering the differences in physical parameters (Table I). The research needed to understand the physics of high current arcs is described under *Needs for Further Research*.

Arc Deflection in a Large DC Furnace

First, the arc deflection angle for a 100.MW DC furnace will be estimated, based on the simplified models described under *Arc Deflection*. For this, transverse magnetic field B, arc jet speed v_z and linear mass density m, which are used in the arc deflection coefficient $D = [IB/(2mv_z^2)]$ in Equation (1) need to be estimated.

For a DC furnace with a current of I = 100 kA and a shell radius of R = 5 m, the horizontal magnetic field at the arc, caused by the buswork shown in Figure 2, would be approximately $B_y = \mu oI/2\pi R \approx 50$ Gauss, assuming no shielding from iron in the shell or unmelted scrap. The maximum arc jet velocity can be estimated from Equation (2). For a typical arc current density at the cathode of 3×10^7 A/m², the arc radius at the cathode would be $r_c \approx 3$ cm. For an arc density of $\rho \approx 1.7 \times 10^{-2}$ kg/m³ corresponding to atmospheric pressure at 10,000°C, the maximum arc jet velocity would be [from Equation (2)] $v_{z,\,max} \approx$ 7,000 m/second. This is probably too high, since the measured arc jet speed was only ≈ one-tenth of the estimate based on Equation (2), and since this is about five times the sound speed at this temperature. Thus assumed is an average jet speed of 1,000 m/second and an arc of average diameter 10 cm, which is similar to that measured previously in high current arcs.[1, 2]

Therefore, the 100 kA arc should have the parabolic shape of Equation (1) with $D = [IB/(2mv_z^2)] = [(100\text{ kA}) \cdot (50 \times 10\text{–}4\text{ T})] / [2 \cdot (1 \times 10^{-4}\text{ kg/m}) \cdot (10^3\text{ m/second})^2] \approx 1\text{ m}^{-1}$. Thus, if the arc has a vertical height of 1 m, it should have a horizontal deflection of about 1 m at the anode (i.e., its deflection angle should be ≈ 45 degrees). This appears to be similar to angles believed to occur in some large furnaces.

For other DC arc furnaces, the arc deflection coefficient D can be estimated from the following approximate scalings: $B \propto I/R$ from simple magnetics, $m \propto I^{1/2}$ for arcs at fixed current density and temperature at atmospheric pressure, and $v_z \propto I^{1/2}$ from Equation (2) for a fixed current density at the cathode spot, implying $D \propto I^{1/2}/R$. Thus, the arc deflection at the anode, caused by the magnetic fields from external buswork, would tend to be largest in furnaces with high current in which the buswork was close to the arc and would increase as the square

of the arc length, according to the model in Equation (1).

Effect of Magnetic Materials on Arc Deflection

A permeable iron shell in an industrial scale DC furnace could significantly reduce the magnetic field because of the buswork at the location of the arc. The magnetic shielding effect of permeable iron can be roughly estimated using a simple one-dimensional model, assuming complete saturation of the iron at B = 10 kG. The thickness of iron needed to shield the magnetic flux from a field of 50 Gauss extending over a length of 5 m from the buswork would be ≈ (50 G/10,000 G) • 5 mm ≈ 2.5 cm. This is similar to the thickness of large furnace shells. Therefore, the existing iron shells should have a significant influence on the estimate of arc deflection shown under *Arc Deflection in a Large DC Furnace*. The magnetic field at the arc would be a complicated function of buswork routing and the leakage of magnetic field through the various holes in the shell.

The scrap iron and steel inside the furnace will most likely shield the magnetic field of the buswork from the arc during the initial meltdown, but only when the temperature of the scrap is below the Curie temperature (≈ 700°C), above which it becomes non-magnetic. Below this temperature, the magnetization of the scrap, by the currents inside the furnace, would probably dominate the arc behavior and cause random deflections of the arc. However, these deflections would probably not reach or damage the refractory wall.

Possible Methods to Control DC Arc Deflection

The simplest way to control arc deflection is to apply a horizontal magnetic field, similar to the experiments described under *Arc Deflection*. Two pairs of magnetic coils 90 degrees apart outside the furnace shell could null out arc deflection in any direction, assuming the effect of the iron shell was taken into account properly. Current for these coils can be tapped from the arc power supply, and their power consumption should be comparable to the rest of the buswork. A second strategy would be to thicken the soft iron shell to ensure that any stray magnetic field caused by the buswork did not penetrate into the furnace.

A third strategy would be to somehow increase the arc mass density or arc jet speed, since both enter into the deflection coefficient D in Equation (1). For a given arc current, the arc jet speed might be increased by reducing the radius of the cathode spot, which could possibly be done by increasing the current density emitted at the cathode surface using a different cathode composition. The arc density might be increased by reducing the arc temperature (e.g., by introducing more cold gas near the cathode spot). The effect of the foamy slag around the arc might also be considered as an indirect means to increase the effective mass density of the arc.

Arc Deflection in AC Furnaces

Note that the arc deflection formula Equation (3) is valid on time scales long compared with the transit time of the arc jet between the cathode and anode, which is ≈ 1 msec for an EAF arc of length ≈ 1 m at an estimated arc speed of 1,000 m/second. Therefore, this model should also be valid for arcs in three-phase AC furnaces.[21] However, in that case, the dominant transverse magnetic field for a given arc would be from the other two electrodes, which are much closer to any given arc. Thus, the AC arc deflection vs. time could be modeled fairly easily based on analysis similar to that leading to Equation (1).

Cathode Spot Instability Model Applied to Large DC Furnaces

Assume that a DC arc furnace of 100 kA has an arc jet speed of $v_z \approx 1{,}000$ m/second, a cathode spot radius of $r_c \approx 3$ cm and an arc length of L ≈ 1 m (see *Arc Deflection in a Large DC Furnace*). According to the model under *Arc Instability*, if the cathode spot motion has a radius of $a \approx r_c \approx 3$ cm (i.e., similar to their relationship in our experiment), and if the instability frequency is 100 Hz, then the arc would have a horizontal velocity of $v_y = \omega a \approx 20$ m/second. Therefore, its position at the anode would move with a radius of $L \cdot (v_y/v_z) \approx 2$ cm. Such a small motion would probably not cause the noise and voltage fluctuations observed in the actual furnaces.

However, a turbulent spectrum of fluctuations is present in EAFs in the range ≈ 10 to 1,000 Hz. At ≈ 10 Hz, the transverse cathode spot velocity would be so slow that the arc would remain perpendicular to the cathode surface. Thus, its location at the anode would probably be determined by the local curvature of the cathode tip. At 1,000 Hz, one axial wavelength of the arc would be between the cathode and the anode, and the horizontal cathode spot speed would be ≈ 200 m/second, corresponding to displacement at the anode of ≈ 20 cm.

It is likely the actual motion of the arc during instability is larger than these estimates, so either the cathode spot movement is larger than assumed previously, or some other physical mechanism is driving arc instability in large furnaces. Cathode spot speeds of up to ≈ 100 m/second and helical (or conical) arc motion have been observed in high current arcs.[1, 6, 16]

Control of Arc Instability in Large Furnaces

If movements of the cathode spot are the main cause of arc instability, as implied by the experiments, then changes in the cathode temperature distribution,

cathode shape or chemical composition could potentially control this instability. Usually large EAFs use ≈ 1 m diameter solid graphite cathodes, which have a cylindrical shape and a hemispherical tip at the arc end.

The most direct means for arc stabilization in this experiment was to increase the diameter of the cathode. However, EAFs at I = 100 kA are unstable, even though the cathode diameter is at least 10 times the cathode spot diameter, in contrast to the experiment at which a 250 A arc was stabilized for a cathode diameter a few times that of the cathode spot diameter. The stabilization in this experiment was attributed to conductive cooling of the surface adjacent to the cathode spot. However, in the industrial furnace, the whole cathode tip may be near 3,500°C because of its immersion inside the furnace. If so, one route to arc stabilization might be to reduce the temperature of the cathode tip, perhaps by moving it nearer to the top of the furnace shell.

Stabilization in this experiment was also seen when the cathode radius was small (i.e., comparable to the cathode spot radius). Thus, another route to arc stabilization in large EAFs might be to reduce the cathode tip diameter to the cathode spot diameter (≈ 6 cm), thus inhibiting the cathode spot motion and arc instability. This might be possible by bundling together many such narrow cathodes into a large multi-tipped cathode, or by forming a single graphite cathode, which would form many separated cathode spots.

Another approach to arc stabilization would be to reduce the cathode spot movement. If this motion is caused by graphite evaporation at the cathode spot, as described part (e) under *Arc Instability*, then the arc instability might be controlled by reducing the evaporation rate of the cathode. This would also increase the lifetime of the cathode, but may be difficult or costly in practice.

Finally, adding an axial magnetic field to an arc could potentially increase its stability, analogously to the stabilization of fusion plasmas. Such a method was proposed and tested on a small-scale experiment.[17] In this case, a weak vertical magnetic field created a new high frequency instability, and a strong vertical magnetic field extinguished the arc.[5] However, such fields have been used in industrial furnaces for stirring the liquid metal bath and may permit some degree of control over arc instability.

Needs for Further Research

Conclusions from these small-scale experiments should not be directly applied to the design of large-scale EAFs without further research, since large industrial arcs have some different physical parameters and a different environment than the small arcs in our experiment. Although some good research has already been done on high current arcs,[1, 2] relatively little is known about the behavior of arcs inside large EAFs, because of their inaccessibility and complexity.

The main parameter differences between our experiment and an industrial arc are summarized in Table I. The arc jet speed is likely to be ≈ 10 to 100 times higher in industrial furnaces. The Mach number of the arc jet may be ≥ 1, which could cause shock waves and significantly modify the arc stability. The hydrodynamic Reynolds number of the industrial arc jet will probably be in the range of $R_H \approx 1{,}000$, making strong turbulence much more likely. In general, the behavior of plasmas with supersonic flow and strong turbulence is not well understood, making this an interesting subject for future research.

The industrial are furnace environment is also considerably more complicated than our experiment, since it contains foamy slag around the arc, unmelted metal scrap and/or splashing liquid metal, convective flows of gases and metal, and uncertain current distributions inside the cathode and liquid metal anode. Each of these factors (and probably many others) can affect arc deflection and instability in the real furnace, and none of them is accounted for in PPPL's model. Therefore, research is needed to identify and model these effects on arc behavior in industrial furnaces.

Another possible difference between the physics of low and high current arcs is the degree to which self-generated magnetic fields can affect the arc behavior, as reflected in the plasma β (ratio of plasma pressure to magnetic pressure) and the magnetic Reynold's number R_M in Table I. Large self-magnetic fields generally cause plasma instability although their effect was probably negligible in this experiment.[5] High current furnace arcs likely have some magnetically self-generated instability, as discussed in the literature.[1, 16, 18]

These small scale arc experiments are completed, but the PPPL would be interested in partnering with industry to continue this research on larger scale furnaces. Progress in such research would depend on the application of state-of-the-art diagnostic and computational tools for measuring and simulating the complicated behavior of the arc plasma, neutral gas and molten metal inside these furnaces.

SUMMARY AND CONCLUSIONS

A set of experiments and modeling was done to understand the arc deflection and instability observed in a I = 250 A DC arc, whereby the graphite cathode and steel anode were meant to simulate the behavior of an industrial scale EAF. The arc deflection, caused by an external magnetic field B, was explained by a simple model of the I × B force on the arc jet. The instability observed in this experiment was explained by the unstable movement of the arc attachment spot at the cathode, rather than by instability of the arc

itself. Some potential applications of these results to industrial scale furnaces were described, but clearly more research is needed before the arc deflection and instability of high current furnaces can be understood and directly controlled.

ACKNOWLEDGMENTS

We wish to thank H.P. Furth, R.C. Davidson and R.J. Goldston of PPPL for supporting this work, which was done under U.S. Department of Energy Contract No. DE-AC02-76-CH03073; for their technical assistance, A. Brooks, P. Heitzenroder, L. Roquemore and L. Zakharov of PPPL; for helpful discussions, P.M. Bellan, G. Bendzsak, B. Bowman, J. Heberlein and S.-E. Stenkvist. Finally, we thank the representatives of ABB and the operators of Charter Steel for permitting us to visit their furnace.

References

1. B. Bowman, "Properties of Arcs in DC Furnaces," *Electric Furnace Conference Proceedings*, Vol. 52, 1994, p. 111.
2. G.R. Jones, "High Pressure Arcs in Industrial Devices: Diagnostic and Monitoring Techniques," Cambridge University Press, Cambridge, 1988.
3. E. Pfender, "Electric Arcs and Arc Gas Heaters," in *Gaseous Electronics, Vol. 1: Electrical Discharges, Chapter 5*, Academic Press, N.Y., 1978.
4. R.J. Hawryluk, *Rev. Modern Physics*, Vol. 70, 1998, p. 537.
5. M. Karasik, "Driven Motion and Instability of an Atmospheric Pressure Arc," Ph.D. Thesis, Princeton University (January 2000), available as PPPL Report No. 3398 (1999), at www.pppl.gov.
6. N. Ao and M. Nakai, "Prevention of Arc Deflection and Electromagnetic Stirring in DC Arc Furnaces," *SEAISI Quarterly*, 1994, p. 20.
7. G. Speckhofer and H.P. Schmidt, "Experimental and Theoretical Investigation of High Pressure Arcs – Part II: The Magnetically Deflected Arc (three-dimensional modeling)," *IEEE Trans. Plasma Sci.*, 1996, 24(4), p. 1,239.
8. G.J. Bendzsak and E.G. Mueller, "Steel Bath Circulation and Arc Deflection in DC Furnaces," *Modern Steelmaking and Casting Techniques*, p. 137.
9. M. Karasik, A.L. Roquemore and S.J. Zweben, "Experiments and Modeling of an Atmospheric Pressure Arc in Applied Oscillating Magnetic Field," *Physics of Plasmas*, Vol. 7, 2000, p. 2,715.
10. J.F. Lancaster, ed. "The Physics of Welding," Pergamon Press, 2nd Edition, 1986.
11. H. Maecker, "Plasma Streaming in Arcs Due to Self-Magnetic Compression," Z. fur Physik 141, 198, 1955; also, "Principles of Arc Motion and Displacement," IEEE Proceedings, 59(4), 1971, p. 439.
12. Y. Raiser, Gas Discharge Physics, Springer-Verlag, New York, 1991.
13. D.H. McQueen, "Noise From Electric Arc Furnaces I: General Considerations," *Scandinavian Journal of Metallurgy*, 7, 5, 1978.
14. S.-E. Stenkvist, "Single Electrode DC Arc Furnace," *Iron and Steel Engineer*, 62, 50, 1985; also, S.-E. Stenkvist and B. Bowman, "High-Power, Graphite Cathode DC Arc Plasma – Properties and Practical Applications for Steelmaking and Ferroalloys Processing," Ch. 8B, Plasma Technology in Metallurgical Procession, p. 103, J. Feinman, Ed., Published by the Iron & Steel Society, Warrendale, Pa., 1987.
15. B. Bowman, G.R. Jordan and F. Fitzgerald, " The Physics of High Current Arcs," *J. of Iron & Steel Society*, 1969, p. 798.
16. G.R. Jordan, B. Bowman and D. Wakelam, "Electric and Photographic Measurements of High Powered Arcs," *J. Phys. D: Applied Phys. 3:1089*, 1970.
17. P.M. Bellan and J.W. Higley, *IEEE Trans.* Plasma Sci. 20, 1992, p. 1,026.
18. K. Ragaller, Z. Naturforsch, 29a, 1974, 556.
19. P.E. King, T.L. Ochs and A.D. Hartman, *J. Appl. Phys.*, 76, 1994, p. 2,059.
20. M. Karasik and S.J. Zweben, "Experiments and Modeling of an Instability of an Atmospheric Pressure Arc," *Physics of Plasmas*, Vol. 7, 2000, p. 4,326.
21. H.L. Larsen, G. Saevarsdottir and J.A. Bakken, "Simulation of AC Arcs in the Silicon Metal Furnace," *Electric Furnace Conference Proceedings*, Vol. 54, 1996, p. 157.